ARTICLES
https://doi.org/10.1038/s41592-020-0774-3

nature methods

Check for updates

RecV recombinase system for in vivo targeted optogenomic modifications of single cells or cell populations

Shenqin Yao[1,8], Peng Yuan[2,8], Ben Ouellette[1], Thomas Zhou[1], Marty Mortrud[1], Pooja Balaram[1], Soumya Chatterjee[1], Yun Wang[1], Tanya L. Daigle[1], Bosiljka Tasic[1], Xiuli Kuang[3], Hui Gong[4], Qingming Luo[4], Shaoqun Zeng[4], Andrew Curtright[5], Ajay Dhaka[5], Anat Kahan[6], Viviana Gradinaru[6], Radosław Chrapkiewicz[2], Mark Schnitzer[2], Hongkui Zeng[1] and Ali Cetin[1,2,5,7] ✉

Brain circuits comprise vast numbers of interconnected neurons with diverse molecular, anatomical and physiological properties. To allow targeting of individual neurons for structural and functional studies, we created light-inducible site-specific DNA recombinases based on Cre, Dre and Flp (RecVs). RecVs can induce genomic modifications by one-photon or two-photon light induction in vivo. They can produce targeted, sparse and strong labeling of individual neurons by modifying multiple loci within mouse and zebrafish genomes. In combination with other genetic strategies, they allow intersectional targeting of different neuronal classes. In the mouse cortex they enable sparse labeling and whole-brain morphological reconstructions of individual neurons. Furthermore, these enzymes allow single-cell two-photon targeted genetic modifications and can be used in combination with functional optical indicators with minimal interference. In summary, RecVs enable spatiotemporally precise optogenomic modifications that can facilitate detailed single-cell analysis of neural circuits by linking genetic identity, morphology, connectivity and function.

The mammalian brain is one of the most complex biological systems. It comprises millions to billions of cells[1] with diverse characteristics. To understand this complexity, it will be essential to define cell types based on properties such as gene expression, morphology and physiology. Furthermore, the unique properties of individual cells need to be related to their connectivity patterns and their activities in a behavioral context. Anatomical information combined with genetic identity and functional properties at the single-cell level will enable better analysis of brain circuitry underlying complex behaviors in health and disease.

A powerful approach to characterizing cell types in the mouse and studying their functions relies on genetics[2]. Using transgenic or viral expression of recombinases allows specific genetic modification[3–5]. Further improvements on spatiotemporal control can achieve even higher-resolution manipulations and studies of biological systems.

Currently, finding individual cells in vivo, characterizing their function and genetically manipulating them in a targeted manner is difficult. The state-of-the-art approach for introducing an exogenous gene to a specific neuron is either by the patch clamp technique[6] or via single-cell electroporation[7,8]. These techniques are challenging and usually result in low and variable yields. Sparse neuronal labeling or manipulation can be achieved by lowering the dose of inducers (for example, tamoxifen, in the case of CreER) or by employing 'inefficient' recombinase reporters (for example, MADM (ref. [9])) to control recombination. However, the sparse genetic modification achieved with these methods is random and difficult to direct to specific cells of interest.

Using optical methods to access and genetically modify individual neurons will offer improvement over the current state-of-the-art methods. Multi-photon interactions with proteins can generate a spatiotemporally restricted excitation[10]. Thus, modifying current genomic manipulation enzymes to make them light-inducible can be a superior approach to reach a high spatiotemporal resolution for targeted single-cell manipulations.

Light-inducible protein-based systems were developed to control protein states, protein localization, transcription and genetic alterations in a spatiotemporal manner[11–35]. Several light-inducible site-specific DNA recombinases (SSRs) have been previously reported[32–36], paving the path for precision single-cell targeting. Magnets, which are variants of the fungal photoreceptor Vivid (VVD) that heterodimerize, were used to generate light-inducible Cre recombinase systems[13,33], and recently a light-inducible Flp recombinase system[35]. Optimized cryptochrome-based light-inducible Cre recombinases have been generated[32], as have wild-type phytochrome-based versions with similar designs[36]. However, optical manipulation of genomes—optogenomics—of individually targeted single cells had not yet been demonstrated in vivo. We developed and validated light-inducible SSR systems named RecVs. In contrast to other light-inducible systems, RecVs induce robust genomic modifications with minimal background recombination under uninduced conditions at different genomic locations and in

[1]Allen Institute for Brain Science, Seattle, WA, USA. [2]CNC Program, Stanford University, Palo Alto, CA, USA. [3]School of Optometry and Ophthalmology, Wenzhou Medical College, Wenzhou, China. [4]Britton Chance Center for Biomedical Photonics, Wuhan National Laboratory for Optoelectronics, Huazhong University of Science and Technology, Wuhan, China. [5]Department of Biological Structure, University of Washington, Seattle, WA, USA. [6]Division of Biology and Biological Engineering, California Institute of Technology, Pasadena, CA, USA. [7]Present address: CNC Program, Stanford University, Palo Alto, CA, USA. [8]These authors contributed equally: Shenqin Yao, Peng Yuan. ✉e-mail: alic@stanford.edu

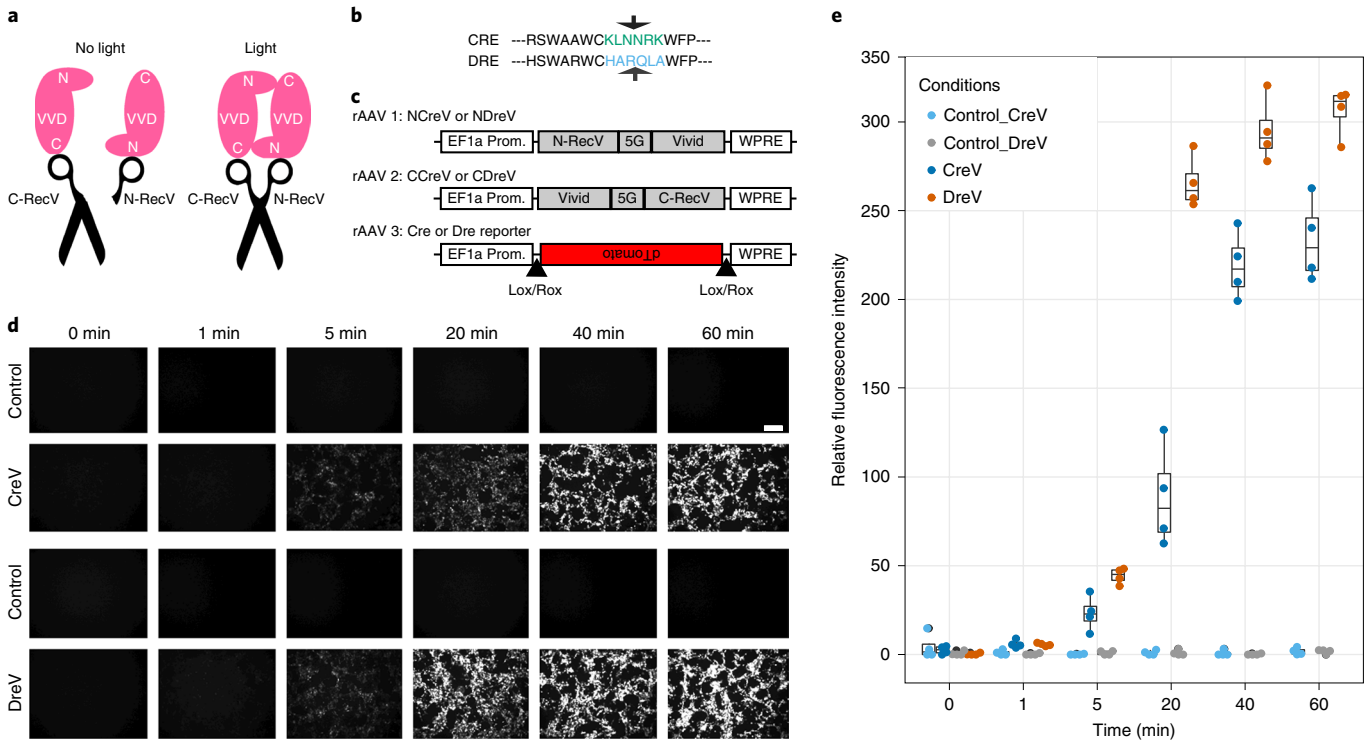

Fig. 1 | Design of the RecV systems. a, Schematic of the RecV system. **b**, Alignment of amino-acid sequences of Cre and Dre recombinases with split site noted by arrows. **c**, Schematic of the CreV and DreV rAAV constructs and a Cre- or Dre-dependent red fluorescent reporter. **d**, dTomato expression in CreV- or DreV-expressing cells after light induction. Controls were not subjected to illumination but otherwise treated similarly. Images were acquired at 48 h postinduction. Scale bar, 200 µm. Images are representative of three independent experiments. **e**, Quantification of the relative fluorescence intensity of reporter constructs after light-induced recombination by CreV or DreV. Each experiment is represented by four replicates. The line across the box represents the median, the lower and upper hinges correspond to the 25th and 75th percentiles, and the upper and lower whiskers extend from the hinge to the largest or smallest values no further than 1.5 × interquartile range from the hinge.

different species. Our work yielded light-inducible versions of the most commonly used SSRs—Cre, Dre and Flp—that allow population-level or target-specific single-cell-level optogenomic modifications in vivo.

Results

Split VVD-SSRs enable efficient light-inducible site-specific DNA modifications. To spatiotemporally regulate site-specific recombination, we generated a light-inducible genetic switch based on the light-sensitive fungal protein VVD[37] and a split-Cre recombinase[20,38–40] (Supplementary Note and Fig. 1a). Guided by the crystal structures of Cre[41] and VVD[42,43] and Cre split location information[38,39], our design brings together the N and C portions of the Cre recombinase in the correct orientation upon light exposure (Fig. 1b). We fused the N-terminal segment of Cre to the N terminus of one VVD monomer, and the C-terminal segment of Cre to the C terminus of another VVD monomer, which we codon diversified. We cotransfected the resulting rAAV expression constructs[44] NCreV and CCreV along with fluorescent Cre-reporter constructs into HEK293T mammalian cells (Fig. 1c). Light induction resulted in robust recombination of the reporter, in contrast to no-light conditions (Fig. 1d,e). We named this combination of proteins CreV, and the general light-inducible VVD-based recombinase system RecV.

To broaden the capabilities of the RecV approach we modified another SSR, Dre[45], which is homologous to Cre. Dre recombinase recognizes a sequence called Rox[46], which is different from LoxP. This creates a possibility to develop Cre and Dre intersectional strategies to further refine cell-type-specific genetic manipulation. We reasoned that the sequence homology between Cre and Dre might be used to generate a split Dre (Fig. 1b). Accordingly, we designed NDreV and CDreV constructs—split at the sequence homologous to Cre split site—and tested them using fluorescent Dre reporter plasmids (Fig. 1c and Supplementary Fig. 1). Our results indicate that light-induced DreV recombination is efficient using one-photon (1P) excitation similar to CreV (Fig. 1d,e), and can also be achieved using two-photon (2P) excitation (Supplementary Fig. 2).

Comparison of single RecV expression constructs with other existing light-inducible recombinase systems. To implement the RecV strategy efficiently and reduce the number of viruses or transgenic mouse lines needed for this system, it is preferable to co-express the two halves of RecVs in a single construct. To achieve this, we tested ways to link the N and C components of CreV and DreV to provide the highest recombination efficiency with the least background recombination (Supplementary Fig. 3a). To generate an efficient co-expression construct, we tested a variety of ways to link the N and C components of CreV or DreV, including internal ribosomal entry site (IRES), ribosomal skipping peptide (2A) and single open reading frames with permutations of the open reading frames; see the Methods section for more details (Supplementary Fig. 3a). We observed the highest efficiencies when we used Cre and Dre split recombinases fused to nuclear localized wild-type VVD and co-expressed with optimized linkers and 2A elements[13,33] (Supplementary Fig. 1). We named the resulting constructs iCreV and iDreV (where i is for improved). The difference between Cre-Magnets[33] and iCreV is that iCreV relies on wild-type VVDs whereas Cre-Magnets use heterodimerizing VVD mutants, with all of the other sequences being equal.

We next compared iCreV and iDreV with versions that use Magnets[13]—we used previously published Cre-Magnet sequences[33] and generated the Dre-Magnets for these comparisons. In HEK293T cells, Magnet-based constructs induced efficient recombination under light conditions; however, they also induced substantial amounts of background recombination without light. In the absence of light, iCreV and iDreV exhibited recombination similar to reporter-only controls and retained high levels of inducibility in the presence of light. iCreV achieved ~1.6-fold higher efficiency than NCreV and CCreV, and iDreV achieved ~0.6-fold lower efficiency than NDreV and CDreV (Supplementary Fig. 3). For both iCreV and Cre-Magnets, we observed efficient recombination in mouse brain slices after light stimulation in vivo. However, using Cre-Magnets without light induction, we observed background recombination throughout the brain (~50 cells per 100-µm-thick coronal slice), whereas iCreV induced no notable recombination (Supplementary Fig. 4).

We also compared the RecV system with a cryptochrome (CRY2)-based light-inducible Cre recombination system[32]. The comparison in HEK293T cells revealed that iCreV performs ~4-fold better than CRY2-based Cre after 60 min of light stimulation. CRY2-based Cre recombination allows only a slight increase (~1.2-fold) over baseline recombination (Supplementary Fig. 3).

Design and screening of light-inducible Flp recombinases. To increase the options for intersectional genomic modifications further, we turned to a third widely used SSR, Flp[47]. There is too little protein sequence similarity between Flp and Cre or Dre to define a split site in Flp based on homology. Thus, we resorted to structure-based de novo design and screening for split sites based on the crystal structure of Flp[48]. Using a more efficient, codon-optimized variant of Flp (FlpO)[49], we split the FlpO coding sequence at 21 loop locations that correspond to transitions between alpha helices and/or beta sheets to lessen the likelihood of altering overall functionality within the split version (Supplementary Fig. 5a). We generated iFlpV constructs following the iCreV design principles and cotransfected HEK293T cells with a Flp-dependent reporter. iFlpV2, 19 and 20 yielded the most notable light-induced recombination with minimal background activity (Supplementary Fig. 5b).

In an effort to further improve the efficiency of light-inducible Flp recombinase activity, we created and tested 62 additional iFlpV variants to scan Flp sites surrounding those of iFlpV2, 19 and 20 (Supplementary Fig. 5c). iFlpV2 remained the most efficient.

RecV mediated light-inducible recombination after whole-brain infection. To test RecV constructs in the entire mouse brain we generated RecV- as well as Cre-expressing rAAVs of the PHP.eB serotype[50]. As a light-independent control, PHP.eB EF1a-Cre virus, when injected either intracerebroventricularly or retro-orbitally into the fluorescent Cre-reporter mice, efficiently and relatively homogeneously infects the entire brain and leads to wide-spread recombination and reporter gene expression (Fig. 2a and Supplementary Fig. 6a).

To test light-inducible recombination using RecVs, first we injected a mixture of PHP.eB NDreV and CDreV viruses into the right ventricle of the Dre-dependent fluorescent reporter mouse, Ai66R. Two weeks later, we exposed the left hemisphere to light. We observed a gradient of recombination from the top of the left hemisphere to deeper structures (Fig. 2b). Sites far away from the light stimulation had no fluorescently labeled cells, except along the intracerebroventricular needle track, where recombination took place, likely due to infection with multiple viral particles. In addition, we tested the iCreV, iDreV and iFlpV constructs with PHP.eB serotype, in SSR-dependent reporter mouse lines. As in our trials with NDreV and CDreV, we observed substantial recombination in the hemisphere exposed to light (Fig. 2c–e and Supplementary Fig. 6b). No notable recombination was observed in iCreV-injected no-light control mice after 4 weeks, demonstrating tight optogenomic control (Supplementary Fig. 6c). These results show that this technique allows specific light-inducible recombination.

Recombinase reporter mouse lines mentioned so far within this section were generated via targeted insertions into the *Rosa26* locus[51]. To test a different locus, we retro-orbitally injected PHP.eB iCreV rAAVs into the Ai167 ChrimsonR reporter mouse line, which has its reporter insertion within the TIGRE locus[52]. We again observed a gradient of recombination from the light-stimulated left hemisphere confirming that other genomic loci in mice can be modified by the RecV system (Supplementary Fig. 6d).

We also tested the feasibility of light-inducible recombination within a deeper brain area, the striatum. With 1P light through an optical fiber we induced local recombination using iCreV in the striatum of Ai162 GCaMP6s Cre reporter mice[52], and recorded changes in fluorescence due to calcium concentration dynamics before and after light stimulation (Supplementary Fig. 7a–d). Due to the localized illumination, GCaMP6s was expressed directly under the fiber, in contrast to the broad expression of red fluorescence from the control virus (Supplementary Fig. 7b). Our results demonstrate that optogenomic modifications can be spatiotemporally regulated within deep brain targets and thereby provide a tool for restricted reporter expression under the optical device in vivo.

Cell-class-specific targeting by intersection of viral RecVs and transgenic recombinases. Versatile and refined cell-type targeting can be achieved by using two or more recombinases with distinct activities[52]. For example, our RecV tools can be combined with existing transgenic recombinase lines and intersectional reporters.

To test the feasibility of this approach, we co-injected PHP.eB iFlpV virus and a PHP.eB Cre/Flp-dependent fluorescent reporter virus into the cortex of mice containing the Rbp4-Cre-KL-100 transgene, which drives Cre expression mostly in layer 5 (L5) excitatory cortical cells. After light stimulation we observed L5-specific reporter gene expression (Fig. 2f), suggesting intersectional specificity.

To provide further evidence that light-mediated intersectional targeting can be achieved in other neuron types, we used the Sst-IRES-FlpO mouse line, which expresses FlpO recombinase selectively in inhibitory somatostatin (Sst) neurons, in conjunction with iCreV. We crossed this mouse line to the Cre/Flp double-dependent fluorescent reporter mouse line Ai65. We retro-orbitally injected the resulting mice with PHP.eB iCreV virus, illuminated the left hemisphere and observed reporter gene expression across multiple cortical layers in sparsely distributed neurons close to the light stimulation site (Fig. 2g). To ascertain that the recombination observed within the light-induced hemisphere is indeed specific to the Sst-positive neurons, we performed immunohistochemistry and confirmed that all of the fluorescently labeled neurons were also labeled with anti-SST antibody staining. Recombination was not detected in the unstimulated hemisphere (Fig. 2g). These results confirm that intersectional control can be achieved by combining virally delivered iFlpV or iCreV with transgenic cell-class-specific Cre or FlpO, respectively.

CreV induces tight light-dependent recombination in zebrafish. To determine whether the RecV system can effectively induce light-dependent recombination in other loci and in organisms other than mice we tested it in zebrafish. We injected NCreV and CCreV constructs into transgenic Zebrabow strain[53] embryos that we reared either in light or in darkness. In this line, Cre recombination induces YFP and/or CFP expression in place of default state RFP expression. One in 24 viable embryos reared in the dark displayed recombination. Of the 37 viable embryos reared in the light, most (32 of 37) had YFP and/or CFP expression, confirming that

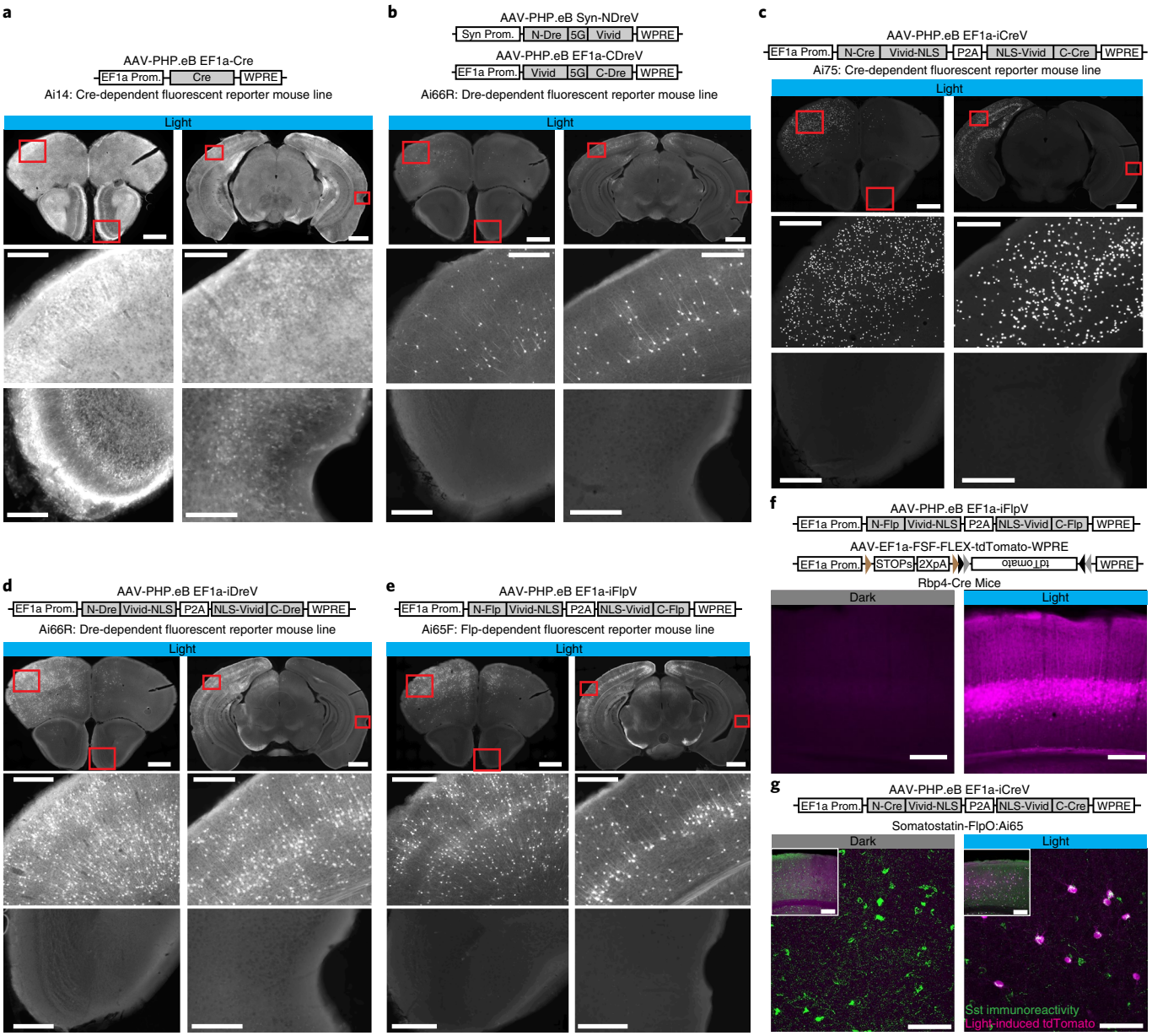

Fig. 2 | Optogenomic modifications with spatiotemporal and cell-class-specific precision in vivo. Reporter mice ($n = 2$ per case) received right hemisphere intracerebroventricular or retro-orbital injection of the indicated PHP.eB rAAVs followed by light stimulation to the left hemisphere 2 weeks postinjection, and imaging 2 weeks post-light stimulation. **a**, tdTomato expression in Ai14 mice injected with AAV-PHP.eB EF1a-Cre; 68,928 and 182,022 cells per section (CPS) were labeled. **b**, tdTomato expression in Ai66R mice ICV injected with a 1:1 mixture of AAV-PHP.eB Syn-NDreV and AAV-PHP.eB EF1a-CDreV; 204 and 608 CPS were labeled. **c**, Nuclear-localized tdTomato expression in Ai75 mice ICV injected with AAV-PHP.eB EF1a-iCreV; 1,323 and 3,649 CPS were labeled. **d**, Ai66R mice were ICV injected with AAV-PHP.eB EF1a-iDreV (1,630 and 2,670 CPS). **e**, tdTomato reporter Ai65F mice were ICV injected with AAV-PHP.eB EF1a iFlpV. Scale bars (**a**–**e**), 1 mm for top images, 200 μm for bottom images (1,386 and 2,471 CPS). **f**, L5 pyramidal neuron-specific Rbp4-Cre mice were locally injected with a mixture of AAV-PHP.eB EF1a-iFlpV and AAV-PHP.eB EF1a-FSF-FLEX-tdTomato. Scale bars, 250 μm (469 of 478 cells in L5). **g**, Somatostatin FlpO mouse line, Sst-IRES-FlpO, crossed with a Cre/Flp double-dependent tdTomato reporter mouse line, Ai65, was retro-orbitally injected with AAV-PHP.eB EF1a-iCreV and light was delivered to the left hemisphere. Recombination was observed in somatostatin-positive inhibitory interneurons as revealed by immunohistochemistry (100% of reporter positive cells (119) were Sst positive (313); 38.1% of Sst cells were reporter positive). Scale bars, 250 μm for inset and 75 μm for zoomed images. All in vivo light activation was applied through the skull on the left hemisphere (opposite intracerebroventricular injection sites in those cases). For **a**–**e**, two coronal planes are shown for each injection (top row) with enlarged views (lower two rows) for areas indicated by red boxes. ICV, intracerebroventricularly.

CreV-induced recombination was light-dependent. We observed recombination in diverse tissues including muscle, skin, heart and spinal cord neurons, and in non-neuronal cells, hindbrain, trigeminal ganglion, Rohon–Beard sensory neurons and hair cells of the lateral line (Fig. 3a–f).

RecV-mediated sparse labeling enables whole-brain reconstructions of single-neuron morphologies. Cre-mediated in vivo reporter expression using the Ai139 mouse line results in strong expression of EGFP in multiple cortical layers[52]. We tested whether light applied to NCreV and CCreV virus-injected Ai139 mice

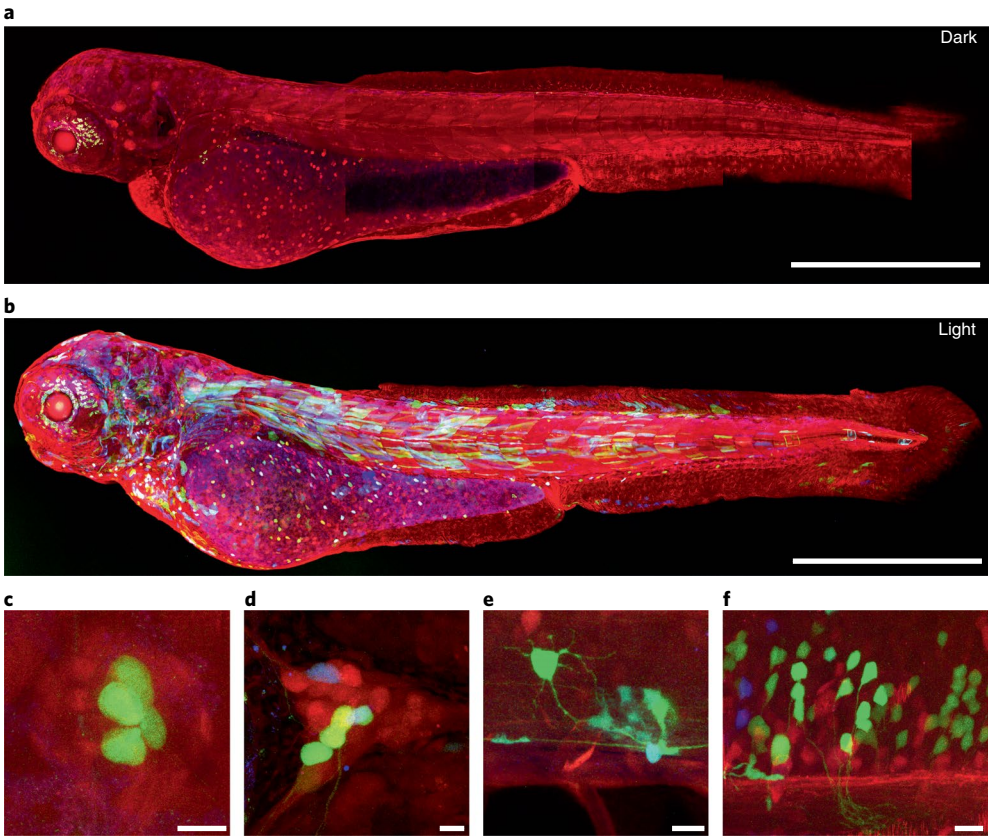

Fig. 3 | CreV allows optogenomic modifications in multiple tissues of *Danio rerio*. a, Confocal images of dark-reared Zebrabow zebrafish larva (3 d postfertilization) co-injected with NCreV and CCreV plasmids. In the default state, RFP is expressed in all cells. Apparent green signal is due to autofluorescence; images are representative of 23 experiments. **b**, Confocal images of a Zebrabow larva co-injected with NCreV and CCreV plasmids and immediately exposed to light; images are representative of 32 experiments. CreV-mediated recombination is reflected as expression of YFP and CFP. **c**–**f**, Higher-magnification images of lateral line hair cells (**c**), trigeminal ganglion (**d**), spinal neuron and glial cells (**e**), and hindbrain neurons (**f**). Scale bars, 500 µm (**a**,**b**), 10 µm (**c**–**f**).

induced sparse yet strong expression at the single-cell level, enabling whole-brain reconstruction of single-neuron morphologies.

With fluorescence micro-optical sectioning tomography (fMOST)[54], we found that low doses of NCreV and CCreV viruses and 3–5 min of light induction yielded sparse and strong labeling of individual neurons in this line (Supplementary Fig. 8). This sparse labeling enabled tracing of axons from many individual neurons. In an example brain, we manually reconstructed eight primary somatosensory cortical neurons (Fig. 4 and Supplementary Videos 1 and 2). These included three L2/3 pyramidal cells (PCs) with ipsilateral cortico-cortical projections, two L2/3 PCs with contralateral cortico-cortical projections and three L5 thick-tufted PCs with ipsilateral cortico-subcortical projections, revealing distinct axonal projection patterns.

RecVs enable 2P-mediated single-cell-specific targeted optogenomic modifications and combinatorial functional imaging in vivo. In cases where restricted genetic access is difficult with conventional methods, it is conceivable to further confine recombination by precise induction through localized illumination. To demonstrate this, we performed headpost craniotomy and 2P-assisted local laser stimulation experiments in trained, head-fixed Ai139 reporter mice. To achieve sparseness, we co-injected a 1:5 mixture of rAAV iCreV and rAAV tdTomato-expressing viruses into the primary visual cortex. The tdTomato virus was included to guide our light stimulation, as well as to serve as a control of overall infection breadth. Our results indicate that local and sparse labeling of neurons is achievable using this method. Furthermore, due to the strength of the Ai139 reporter expression, individual axons and boutons can be readily visualized without immunohistochemical enhancement at sites far away from neuronal cell bodies, suggesting that these brains could be subjected to whole-neuron reconstruction (Supplementary Fig. 9).

To investigate the feasibility of this approach at the single-cell level, we tested 2P illumination in combination with iCreV. In 2P-targeted cortical cells of Ai14 reporter mice, we elicited Cre-dependent gene expression with single-cell precision in vivo (Fig. 5a,b). In many cases, we observed reporter expression in the target cell but not in the inducible cells next to it (Fig. 5c and Supplementary Fig. 10), demonstrating high spatial accuracy. We tested various 2P induction protocols and plotted the probability of iCreV activation against the distance to the target cell in each condition (Fig. 5d). Our results suggest that target cell induction rate increases as more laser power and scan time are applied. However, powerful 2P stimulation in some cases also led to nonspecific induction within a 10-µm radius of the target cell (as high as 18%). Cells within a 10–50-µm radius from the target cell showed a baseline induction rate of 6–7%. The induction rate in no-light conditions was low (~3% on average; Supplementary Fig. 11).

We next tested the feasibility of combining calcium imaging with the iCreV system. We co-injected iCreV and GCaMP7f (ref. [55]) viral constructs into Ai14 mouse cortex. We measured the induction probability of iCreV after 30 min of calcium imaging. The 920-nm excitation provided good-quality jGCaMP7f

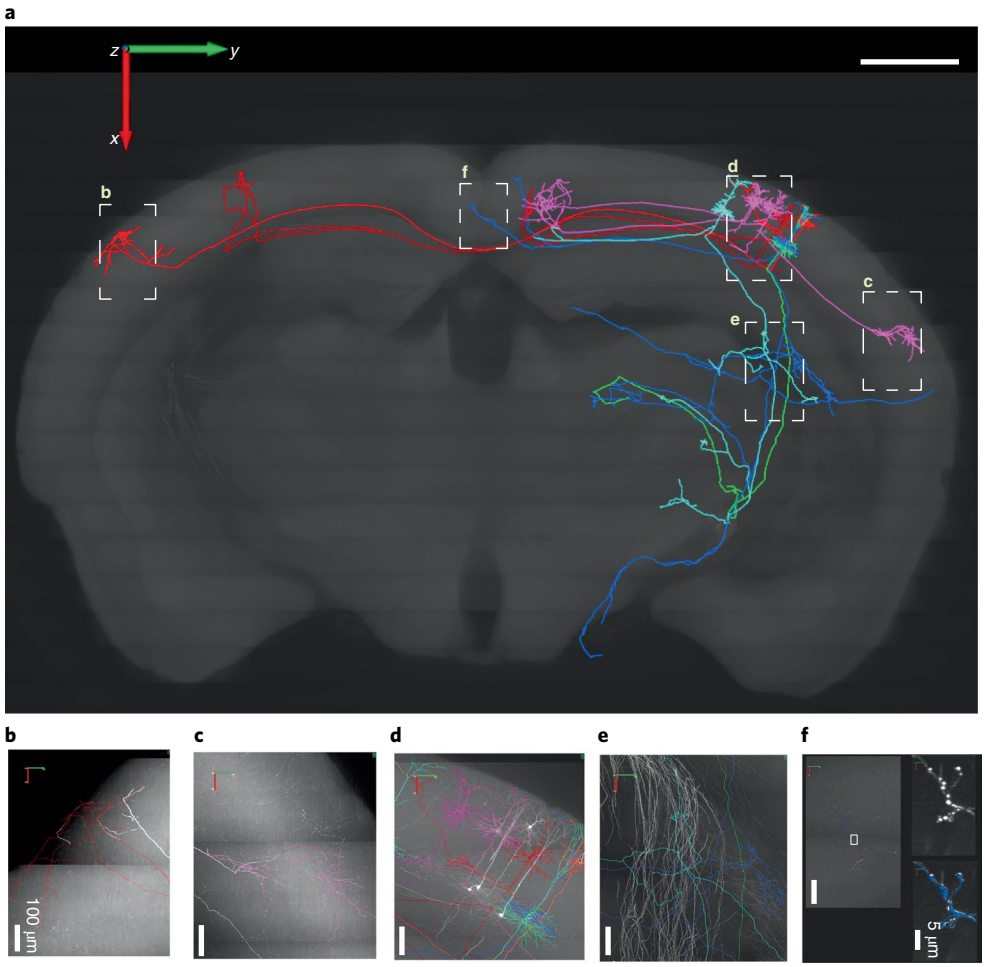

Fig. 4 | Cortical PCs labeled RecVs and were reconstructed at the whole-brain level. a, Eight reconstructed PCs in a mouse somatosensory cortex include three layer-2/3 PCs (in pink) with ipsilateral cortico-cortical projections, two layer-2/3 PCs (in red) with contralateral cortico-cortical projections and three L5 thick-tufted PCs (one green, one blue, one light blue) with ipsilateral cortico-subcortical projections. Local axonal clusters are incomplete because labeling at the somata region is too dense in this brain for tracing fine axonal branches. The eight reconstructed PCs are superimposed onto a coronal brain plane located 5,201–5,400 μm posterior to the olfactory bulb (scale bar, 1 mm). Five Ai139 EGFP reporter mice received local virus injection and light stimulation, and whole-brain neuronal reconstruction was performed using the fMOST images from one mouse that received 5 min of light stimulation. **b**–**f**, Enlarged views of areas outlined by dashed boxes in **a**, with reconstructions (in colors) superimposed on original images with EGFP fluorescence shown as white. In **f**, the two panels on the right (without reconstruction in white, with reconstruction in blue) are enlarged views of the boxed area in the left panel, showing the high-resolution details of a segment of axon with enlarged boutons. The whole-brain image stack is composed of 12,089 images; resolution of *xyz*, $0.3 \times 0.3 \times 1\,\mu m^3$.

signal; however, it was also potent in activating the iCreV system (close to 100%). To reduce iCreV induction during the imaging session, we tested longer-wavelength excitation of jGCaMP7f at 1,000, 1,010 and 1,040 nm. At these wavelengths, the induction of iCreV was substantially reduced, with moderately reduced jGCaMP7f signals (Fig. 5e–g). This allows functional imaging of cells with minimal interference to subsequent light-inducible optogenomic modifications.

Discussion

Light-inducible Cre recombinases have been reported previously[32–34,36]. Magnet-based light-inducible Cre recombination is efficient in mammalian cells, but it also has background in vitro and in vivo compared with its VVD-based counterpart. In a screen to generate a light-inducible FlpO, we discovered a Flp split site (S27-to-G28) that yielded efficient dimerization-induced recombination. Independent discovery of this site was reported in a recent study[35].

The demonstration of the intracerebroventricular route for whole-brain infections using PHP.eB AAV virus may prove valuable in many scenarios. Brains of embryos might be injected via this route to avoid damage to the eye. In multiple mammalian species, this approach may further promote infection of the nervous system and overcome some obstacles related to intravenous delivery of viruses. It may also help avoid immune-response interference with infections. Therefore, it may be useful for gene therapy.

RecV technology may enable loss- or gain-of-function studies by switching genes off or on, followed by monitoring effects on development, physiology or behavior. This may provide more refined spatiotemporal specificity than current pharmacologically gated genetic approaches[56] (for example, CreER or tTA systems). Spatiotemporally restricted single-cell-targeted 2P induction combined with previous functional characterization by imaging can provide a powerful means to interrogate cell ensembles. While we demonstrated the single-cell accuracy of the iCreV system, practical variables (for example, movement of tissue during induction, ambient light or high multiplicity of infection) may reduce the accuracy. In model systems where germline modification is not available or prohibitively expensive, specificity may be achieved by integrating

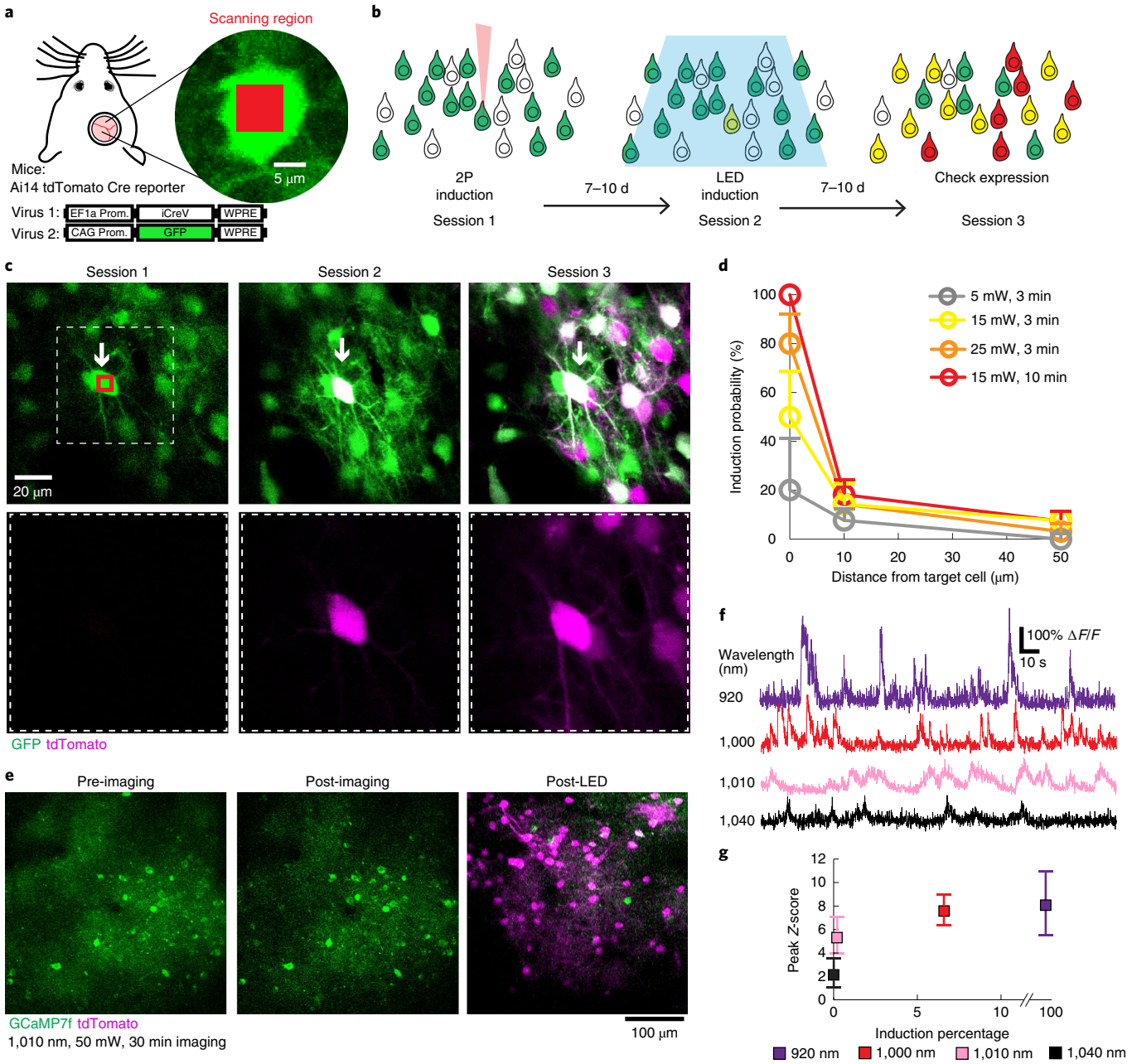

Fig. 5 | 2P-guided targeted single-cell optogenomic modifications by iCreV in mouse neocortex. a, Diagram of in vivo experiment. Inset shows laser induction area (red square) in target cell (green) within mouse's craniotomy. Viral vectors and mouse line used are indicated. **b**, Experimental timeline. A month after virus injections, each mouse underwent three imaging sessions with 2P targeted induction (session 1), LED induction (session 2) and a final assessment for expression (session 3). **c**, Example 2P images from a targeted induction. Arrows indicate target cell and red box indicates induction scanning region. Bottom row shows magnified regions (dashed box) containing target cell. Similar results were reproduced in five mice. **d**, Quantification of in vivo 2P induction rates under different scanning protocols at 0-, 10- and 50-μm distance to target cells. $N = 4$, 5, 3 and 5 cells for target cells; 14, 22, 13 and 14 cells for 10-μm distance; and 93, 122, 85 and 96 cells for 50-μm distance (all in the order of 5 mW 3 min, 15 mW 3 min, 25 mW 3 min and 15 mW 10 min). Data represent mean with standard error of the proportions. **e**, Representative 2P images before and after 30 min of calcium imaging with 1,000-nm 2P excitation of jGCaMP7f. Similar results were reproduced in three mice. **f**, Example calcium traces from the imaged cortex at different wavelengths. **g**, Quantification of in vivo 2P induction rate after 30 min of calcium imaging under four excitation wavelengths held at 50 mW, and the quality of calcium signal in each condition. Data shown as median, with error bars indicating 25th and 75th percentiles of calcium peak height. $N = 100$ events for all conditions.

RecVs into viral vectors equipped with short cell-type-specific promoters or enhancers[57,58], or by target-defined retrograde infection[59].

Overall, the broad range of potential applications shows that the light-inducible recombinase system presented in this study enables spatiotemporal precision and multiple combinatorial strategies for the micro- and macro-level analyses of neural circuits, as well as many other biological systems, in a variety of organisms.

Online content

Any methods, additional references, Nature Research reporting summaries, source data, extended data, supplementary information, acknowledgements, peer review information; details of author contributions and competing interests; and statements of data and code availability are available at https://doi.org/10.1038/s41592-020-0774-3.

Received: 13 January 2018; Accepted: 11 February 2020;
Published online: 23 March 2020

References

1. Herculano-Houzel, S. The human brain in numbers: a linearly scaled-up primate brain. *Front. Hum. Neurosci.* **3**, 31 (2009).
2. Huang, Z. J. & Zeng, H. Genetic approaches to neural circuits in the mouse. *Annu. Rev. Neurosci.* **36**, 183–215 (2013).
3. Nagy, A. Cre recombinase: the universal reagent for genome tailoring. *Genesis* **26**, 99–109 (2000).
4. Branda, C. S. & Dymecki, S. M. Talking about a revolution: the impact of site-specific recombinases on genetic analyses in mice. *Dev. Cell* **6**, 7–28 (2004).
5. Glaser, S., Anastassiadis, K. & Stewart, A. F. Current issues in mouse genome engineering. *Nat. Genet.* **37**, 1187–1193 (2005).
6. Velez-Fort, M. et al. The stimulus selectivity and connectivity of layer six principal cells reveals cortical microcircuits underlying visual processing. *Neuron* **83**, 1431–1443 (2014).
7. Marshel, J. H., Mori, T., Nielsen, K. J. & Callaway, E. M. Targeting single neuronal networks for gene expression and cell labeling in vivo. *Neuron* **67**, 562–574 (2010).
8. Rompani, S. B. et al. Different modes of visual integration in the lateral geniculate nucleus revealed by single-cell-initiated transsynaptic tracing. *Neuron* **93**, 767–776 e766 (2017).
9. Luo, L. Fly MARCM and mouse MADM: genetic methods of labeling and manipulating single neurons. *Brain Res. Rev.* **55**, 220–227 (2007).
10. Denk, W., Strickler, J. H. & Webb, W. W. Two-photon laser scanning fluorescence microscopy. *Science* **248**, 73–76 (1990).
11. Shimizu-Sato, S., Huq, E., Tepperman, J. M. & Quail, P. H. A light-switchable gene promoter system. *Nat. Biotechnol.* **20**, 1041–1044 (2002).
12. Levskaya, A., Weiner, O. D., Lim, W. A. & Voigt, C. A. Spatiotemporal control of cell signalling using a light-switchable protein interaction. *Nature* **461**, 997–1001 (2009).
13. Kawano, F., Suzuki, H., Furuya, A. & Sato, M. Engineered pairs of distinct photoswitches for optogenetic control of cellular proteins. *Nat. Commun.* **6**, 6256 (2015).
14. Muller, K. et al. A red/far-red light-responsive bi-stable toggle switch to control gene expression in mammalian cells. *Nucleic Acids Res.* **41**, e77 (2013).
15. Lungu, O. I. et al. Designing photoswitchable peptides using the AsLOV2 domain. *Chem. Biol.* **19**, 507–517 (2012).
16. Crefcoeur, R. P., Yin, R., Ulm, R. & Halazonetis, T. D. Ultraviolet-B-mediated induction of protein–protein interactions in mammalian cells. *Nat. Commun.* **4**, 1779 (2013).
17. Strickland, D. et al. TULIPs: tunable, light-controlled interacting protein tags for cell biology. *Nat. Methods* **9**, 379–384 (2012).
18. Kennedy, M. J. et al. Rapid blue-light-mediated induction of protein interactions in living cells. *Nat. Methods* **7**, 973–975 (2010).
19. Motta-Mena, L. B. et al. An optogenetic gene expression system with rapid activation and deactivation kinetics. *Nat. Chem. Biol.* **10**, 196–202 (2014).
20. Wang, X., Chen, X. & Yang, Y. Spatiotemporal control of gene expression by a light-switchable transgene system. *Nat. Methods* **9**, 266–269 (2012).
21. Bugaj, L. J., Choksi, A. T., Mesuda, C. K., Kane, R. S. & Schaffer, D. V. Optogenetic protein clustering and signaling activation in mammalian cells. *Nat. Methods* **10**, 249–252 (2013).
22. Nihongaki, Y., Yamamoto, S., Kawano, F., Suzuki, H. & Sato, M. CRISPR-Cas9-based photoactivatable transcription system. *Chem. Biol.* **22**, 169–174 (2015).
23. Lee, S. et al. Reversible protein inactivation by optogenetic trapping in cells. *Nat. Methods* **11**, 633–636 (2014).
24. Dagliyan, O. et al. Engineering extrinsic disorder to control protein activity in living cells. *Science* **354**, 1441–1444 (2016).
25. Gasser, C. et al. Engineering of a red-light-activated human cAMP/cGMP-specific phosphodiesterase. *Proc. Natl Acad. Sci. USA* **111**, 8803–8808 (2014).
26. Wu, Y. I. et al. A genetically encoded photoactivatable Rac controls the motility of living cells. *Nature* **461**, 104–108 (2009).
27. Strickland, D., Moffat, K. & Sosnick, T. R. Light-activated DNA binding in a designed allosteric protein. *Proc. Natl Acad. Sci. USA* **105**, 10709–10714 (2008).
28. Lee, J. et al. Surface sites for engineering allosteric control in proteins. *Science* **322**, 438–442 (2008).
29. Polstein, L. R. & Gersbach, C. A. A light-inducible CRISPR-Cas9 system for control of endogenous gene activation. *Nat. Chem. Biol.* **11**, 198–200 (2015).
30. Konermann, S. et al. Optical control of mammalian endogenous transcription and epigenetic states. *Nature* **500**, 472–476 (2013).
31. Yazawa, M., Sadaghiani, A. M., Hsueh, B. & Dolmetsch, R. E. Induction of protein–protein interactions in live cells using light. *Nat. Biotechnol.* **27**, 941–945 (2009).
32. Taslimi, A. et al. Optimized second-generation CRY2-CIB dimerizers and photoactivatable Cre recombinase. *Nat. Chem. Biol.* **12**, 425–430 (2016).
33. Kawano, F., Okazaki, R., Yazawa, M. & Sato, M. A photoactivatable Cre-loxP recombination system for optogenetic genome engineering. *Nat. Chem. Biol.* **12**, 1059–1064 (2016).
34. Schindler, S. E. et al. Photo-activatable Cre recombinase regulates gene expression in vivo. *Sci. Rep.* **5**, 13627 (2015).
35. Jung, H. et al. Noninvasive optical activation of Flp recombinase for genetic manipulation in deep mouse brain regions. *Nat. Commun.* **10**, 314 (2019).
36. Hochrein, L., Mitchell, L. A., Schulz, K., Messerschmidt, K. & Mueller-Roeber, B. L-SCRaMbLE as a tool for light-controlled Cre-mediated recombination in yeast. *Nat. Commun.* **9**, 1931 (2018).
37. Loros, J. J. & Dunlap, J. C. Genetic and molecular analysis of circadian rhythms in *Neurospora*. *Ann. Rev. Physiol.* **63**, 757–794 (2001).
38. Hirrlinger, J. et al. Split-Cre complementation indicates coincident activity of different genes in vivo. *PLoS ONE* **4**, e4286 (2009).
39. Jullien, N., Sampieri, F., Enjalbert, A. & Herman, J. P. Regulation of Cre recombinase by ligand-induced complementation of inactive fragments. *Nucleic Acids Res.* **31**, e131 (2003).
40. Wang, P. et al. Intersectional Cre driver lines generated using split-intein mediated split-Cre reconstitution. *Sci. Rep.* **2**, 497 (2012).
41. Guo, F., Gopaul, D. N. & van Duyne, G. D. Structure of Cre recombinase complexed with DNA in a site-specific recombination synapse. *Nature* **389**, 40–46 (1997).
42. Vaidya, A. T., Chen, C. H., Dunlap, J. C., Loros, J. J. & Crane, B. R. Structure of a light-activated LOV protein dimer that regulates transcription. *Sci. Signal.* **4**, ra50 (2011).
43. Zoltowski, B. D. et al. Conformational switching in the fungal light sensor Vivid. *Science* **316**, 1054–1057 (2007).
44. Cardin, J. A. et al. Driving fast-spiking cells induces gamma rhythm and controls sensory responses. *Nature* **459**, 663–667 (2009).
45. Anastassiadis, K. et al. Dre recombinase, like Cre, is a highly efficient site-specific recombinase in *E. coli*, mammalian cells and mice. *Dis. Model. Mech.* **2**, 508–515 (2009).
46. Sauer, B. & McDermott, J. DNA recombination with a heterospecific Cre homolog identified from comparison of the pac-c1 regions of P1-related phages. *Nucleic Acids Res.* **32**, 6086–6095 (2004).
47. Andrews, B. J., Proteau, G. A., Beatty, L. G. & Sadowski, P. D. The FLP recombinase of the 2μ circle DNA of yeast: interaction with its target sequences. *Cell* **40**, 795–803 (1985).
48. Chen, Y., Narendra, U., Iype, L. E., Cox, M. M. & Rice, P. A. Crystal structure of a Flp recombinase–Holliday junction complex: assembly of an active oligomer by helix swapping. *Mol. Cell* **6**, 885–897 (2000).
49. Raymond, C. S. & Soriano, P. High-efficiency FLP and PhiC31 site-specific recombination in mammalian cells. *PLoS ONE* **2**, e162 (2007).
50. Chan, K. Y. et al. Engineered AAVs for efficient noninvasive gene delivery to the central and peripheral nervous systems. *Nat. Neurosci.* **20**, 1172–1179 (2017).
51. Soriano, P. Generalized lacZ expression with the ROSA26 Cre reporter strain. *Nat. Genet.* **21**, 70–71 (1999).
52. Daigle, T. L. et al. A suite of transgenic driver and reporter mouse lines with enhanced brain-cell-type targeting and functionality. *Cell.* **174**, 465–480.e422 (2018).
53. Pan, Y. A. et al. Zebrabow: multispectral cell labeling for cell tracing and lineage analysis in zebrafish. *Development* **140**, 2835–2846 (2013).
54. Gong, H. et al. High-throughput dual-colour precision imaging for brain-wide connectome with cytoarchitectonic landmarks at the cellular level. *Nat. Commun.* **7**, 12142 (2016).
55. Dana, H. et al. High-performance calcium sensors for imaging activity in neuronal populations and microcompartments. *Nat. Methods* **16**, 649–657 (2019).
56. Joyner, A. L. & Zervas, M. Genetic inducible fate mapping in mouse: establishing genetic lineages and defining genetic neuroanatomy in the nervous system. *Dev. Dyn.* **235**, 2376–2385 (2006).
57. Dimidschstein, J. et al. A viral strategy for targeting and manipulating interneurons across vertebrate species. *Nat. Neurosci.* **19**, 1743–1749 (2016).
58. Liu, Y. J. et al. Tracing inputs to inhibitory or excitatory neurons of mouse and cat visual cortex with a targeted rabies virus. *Curr. Biol.* **23**, 1746–1755 (2013).
59. Tervo, D. G. et al. A designer AAV variant permits efficient retrograde access to projection neurons. *Neuron* **92**, 372–382 (2016).

Methods

Plasmid and virus construction for RecVs. Sequences of NCre-5G-VVD, VVD-5G-CCre, NCre-5G-VVD-IRES-VVD-5G-CCre, VVD-5G-CCre-IRES-NCre-5G-VVD, NCre-5G-VVD-PQR-VVD-5G-CCre, VVD-5G-CCre-PQR-NCre-5G-VVD, VVD-5G-CDre-IRES-NDre-5G-VVD, NCre-Magnets-NLS-P2A-NLS-Magnets-CCre, NCre-VVD-NLS-P2A-NLS-VVD-CCre, NDre-Magnets-NLS-P2A-NLS-Magnets-CDre, NDre-VVD-NLS-P2A-NLS-VVD-CDre and all iFlpV versions were chemically synthesized (GenScript). The 19–59-amino acid (aa) N terminus and 60–343 C terminus of Cre were used in all CreV cases. To screen poly-cistronic cassettes with the best light-inducible recombinase activity, N and C parts of RecV, as well as IRES-mediated, PQR-mediated and P2A-mediated RecV poly-cistronic cassettes, were cloned into pCDNA3.1 with the CMV promoter (Supplementary Fig. 1).

To generate recombinant AAV viruses expressing split VVD-Cre (CreV) or VVD-Dre (DreV), the N or C parts of CreV or DreV were cloned after the human EF1a promoter, followed by WPRE and hGH-polyA signal (Supplementary Fig. 1). The Cre reporters, pAAV-EF1a-Flex-dTomato or EGFP-WPRE-hGHpA, used pairs of double inverted LoxP and Lox2272 sites to flank the reporter dTomato or EGFP sequence. The Dre reporter, pAAV-EF1a-Frex-dTomato-WPRE-hGHpA, was generated by inserting an inverted dTomato sequence flanked with Rox sites after the human EF1a promoter, followed by WPRE and hGH-polyA signal (Supplementary Fig. 1).

A total of 21 iFlpV variants were generated with custom gene synthesis as follows: iFlpV1: 11-aa N and 412-aa C; iFlpV2: 27-aa N and 396-aa C; iFlpV3: 49-aa N and 374-aa C; iFlpV4: 67-aa N and 356-aa C; iFlpV5 72-aa N and 351-aa C; iFlpV6: 85-aa N and 338-aa C; iFlpV7: 95-aa N and 328-aa C; iFlpV8: 114-aa N and 309-aa C; iFlpV9: 129-aa N and 294-aa C; iFlpV10: 151-aa N and 272-aa C; iFlpV11: 169-aa N and 254-aa C; iFlpV12: 197-aa N and 226-aa C; iFlpV13: 208-aa N and 215-aa C; iFlpV14: 237-aa N and 186-aa C; iFlpV15: 251-aa N and 172-aa C; iFlpV16: 290-aa N and 133-aa C; iFlpV17: 318-aa N and 105-aa C; iFlpV18: 343-aa N and 80-aa C; iFlpV19: 374-aa N and 49-aa C; iFlpV20: 388-aa N and 35-aa C; and iFlpV21: 408-aa N and 15-aa C. Additional iFlpV2 variants were generated spanning amino acids 16–39 and 366–405 covering the entire region, leading to 61 additional constructs. Construct 62 was generated based on iFlpV2 with an addition of the linker GGSGG—which is originally present between the C terminus VVD and FlpV—to also between N terminus FlpV and VVD. These constructs were cloned in pcDNA3.1 mammalian expression plasmids.

AAV1, AAV-DJ and AAV-PHP.eB serotype viruses were produced in house with titers of AAV1-EF1a-NCreV, 1.05×10^{12} genome copies per milliliter; AAV1-EF1a-CCreV, 5.16×10^{12}; AAV1-EF1a-NDreV, 4.20×10^{13}; AAV1-EF1a-CDreV, 5.40×10^{13}; AAV-DJ-EF1a-Cre, 2.00×10^{13}; AAV1-CAG-Flex-EGFP, 1.34×10^{13}; AAV-DJ-EF1a-Frex-dTomato, 1.90×10^{12}, 7.7×10^{11}, 1.6×10^{13}; AAV-PHP.eB-EF1a-Cre, 5.8×10^{13}; AAV-PHP.eB-Syn-NDreV, 4.2×10^{13}; AAV-PHP.eB-EF1a-CDreV, 3.9×10^{13}; PHP.eB iCreV, 2.6×10^{13}; PHP.eB iDreV, 3.3×10^{13}; PHP.eB iFlpV, 2.7×10^{13}; AAV-PHP.eB-EF1a EGFP, 2.03×10^{13}; and AAV- Cre-Magnets, 3.00×10^{13} per ml. AAV5.CAG.tdTomato (1.0×10^{13} genome copies per ml) was purchased from UNC Vector core.

Light activation in cultured cells. HEK293T (ATCC) cells were seeded into six-well plates 1 d before transfection and reached 80% confluency on the day of transfection. Cells were cotransfected with reporters expressing dTomato for Cre, Dre or Flp, for testing Cre-, Dre- or Flp-mediated recombination and various constructs of RecVs. Cells in the control groups were transfected with reporters alone. Each condition contained four replicates. Plates were kept in the dark immediately after transfection. Experimental cells were exposed to blue light 24 h later, and were then kept in the dark immediately after light exposure. Cells were imaged for fluorescent reporter expression 48 h after light induction, using a ×10 objective on an inverted fluorescence microscope. Reporter expression in each condition was quantified using ImageJ. The corrected total fluorescence intensity = integrated density − (area of each image × mean fluorescence of background readings). The mean corrected total fluorescence intensity from four replicates was used to represent the relative fluorescence intensity of each condition. Light inducibility of RecV was calculated as the ratio of the relative fluorescence intensity with light to that without light.

Transcranial cortical in vivo 1P optogenomic modifications. All animal experiments were performed in compliance with Allen Institute for Brain Science Institutional Animal Care and Use Committee (IACUC) guidelines. Stereotaxic injections were performed in adult C57BL/6J (stock no. 00064, The Jackson Laboratory) or transgenic reporter mice with a 1:1:1 or 1:1 mixture of three or two different rAAVs. For all experiments, animals were anesthetized with isoflurane (5% induction, 1.5% maintenance) and placed on a stereotaxic frame (model no. 1900, David Kopf Instruments). An incision was made to expose the skull, including bregma, lambda and the target sites. Stereotaxic coordinates were measured from the bregma and were based on The Mouse Brain in Stereotaxic Coordinates[60,61]. A burr hole was made above the target by thinning the skull using a small drill bit until only a very thin layer remained. An opening was then made using a microprobe, and the remaining thinned skull was gently pulled away. All animals were injected at each target with 500 nl of virus at a rate of ~150 nl min^{-1} using a Nanoject II microinjector (Drummond Scientific). Intraventricular injection of AAV-PHP.eB viruses was conducted by injecting 2 µl of virus into the lateral ventricle using a Nanoject II microinjector. The glass pipettes had inner diameters between 10 and 20 µm.

Unless noted otherwise, 2 weeks following AAV injection, animals were anesthetized and returned to the stereotaxic frame. An incision was made in the previous location to once again reveal the location of the injection sites. A light-emitting diode (LED) light source (LED-64s, Amscope) was mounted to the surgical microscope and positioned 7–10 cm directly above the animal's skull. The amount of time the animal was exposed to light varied with experiments. Small amounts of sterile PBS were periodically applied to the scalp and skull to prevent drying.

Two weeks following light exposure, animals were perfused with 4% paraformaldehyde (PFA). Brains were dissected and postfixed in 4% PFA at room temperature for 3–6 h and then overnight at 4 °C. Brains were then rinsed briefly with PBS and stored in PBS with 10% sucrose solution. Brains were then sectioned at a thickness of 100 µm while frozen on a sliding microtome (Leica SM2010 R). Brain sections were mounted on 2.5×7.5-cm^2 Plus slides and coverslipped with Vectashield with DAPI (H-1500, Vector Laboratories). Slides were then imaged using a ×10 objective on a Leica TCS SP8 confocal microscope (Leica Microsystems) or using a ×10 objective on an epi-fluorescence serial scanning microscope (VS-110, Olympus). In certain cases, images were pseudo-colored to grayscale or magenta for presentation purposes.

The ImageJ trainable WeKa segmentation toolkit was used for image segmentation and cell counting. Two separate classifiers were applied, one for images of reporter mice injected with AAV-PHP.eB EF1a-Cre, which contain dense fluorescent cells, and another for those with sparser fluorescent cells. Six images of 500 × 500 pixels from Ai14 mice injected with AAV-PHP.eB EF1a-Cre virus, and five images of 1,000 × 1,000 pixels from Ai75 mice injected with AAV-PHP.eB EF1a-iCreV, were used to train these two classifiers. The segmented images then underwent automatic thresholding, watershed separation and particle analysis to count the number of cells, followed by manual inspection and correction.

For fMOST imaging, approximately 2 weeks following light exposure, animals were perfused with 4% PFA. Brains were dissected and postfixed in 4% PFA at room temperature for 3–6 h and then overnight at 4 °C. Brains were then transferred to PBS with 0.1% sodium azide for storage at 4 °C until embedding.

Somatostatin immunostaining was conducted using the primary antibody of anti-Somatostatin-28 (1:500, T-4546.0400, Peninsula Laboratories), and the secondary antibody of Alexa Fluor 647 donkey anti-mouse IgG (1:500, 711-605-152, Jackson ImmunoResearch).

Cortical in vivo population 2P optogenomic modifications. All animal experiments were performed in compliance with Allen Institute for Brain Science IACUC guidelines. A titanium head plate was attached to the skull of mice to allow positioning and restraint of the mice during imaging. The hole of the head plate was positioned over visual cortical areas, approximately 2.9 mm posterior and 2.7 mm lateral from the bregma. A 5-mm craniotomy was introduced using a dental drill. The dura was removed, and a multilayer glass coverslip was positioned above the craniotomy. The head plate and coverslips were secured using cyanoacrylate glue and Metabond. After a period of at least 1 week, a dental drill was used to remove the cement and Metabond holding the coverslip in place, and the coverslip was removed. A Dumont Nanoject II was then used to inject 500 nl of viruses into the visual cortex. A new coverslip was placed and adhered. The area above the coverslip was blocked from light using a combination of dental cement and Kwik-cast, both mixed with black acrylic paint powder.

After at least 3 weeks following viral injection, the animal received 2P laser stimulation. Under dark conditions, the Kwik-cast was removed, and the animal's head plate was mounted in position. The injection area was identified by the presence of the EGFP-labeled cells. Laser output was set to 900 nm to optimally induce recombination. A 600×600-μm^2 area was stimulated at three depths (100, 150 and 200 µm) for 15 min each. After stimulation, black Kwik-cast was reapplied. At 2 weeks following stimulation, mice were perfused.

Deep brain in vivo stimulation and imaging. All experiments were performed in compliance with the Caltech Animal Care and Use Committee and Office of Laboratory Animal Resources. For deep brain optogenomic modification and imaging experiments, stereotaxic injections were made into the striatum of 11-week-old Ai162-GC6s (Stock No. 031562, The Jackson Laboratory) Cre-dependent GCaMP6s reporter mice with a 1:1 mixture of PHP.eB.iCreV and a control AAV unconditionally expressing red fluorescent protein (AAV5.CAG.tdTomato). For all experiments, animals were anesthetized with isoflurane (5% induction, 1.5% maintenance) and placed on a stereotaxic frame (942, David Kopf Instruments). An incision was made to expose the skull, including bregma, lambda and the target sites. Stereotaxic coordinates were measured from the bregma and were based on *The Mouse Brain in Stereotaxic Coordinates*[60,61]. A burr hole was made above the target. All animals were injected with 2×400 nl of virus mixture, at two dorsoventral positions, 300 µm apart, at a rate of ~80 nl min^{-1} using an UltraMicroPump (UMP3-4, World Precision Instruments). Following virus injection, an optical fiber with cut length of 5 mm and diameter of 400 µm

(numerical aperture (NA) 0.48, Doric Lenses) was firmly mounted to a stereotaxic holder. The optical fiber was then inserted to the striatum (anteroposterior +1.0 mm, mediolateral ±1.3 mm, dorsoventral −3.5 mm, from either left or right side) through a craniotomy and positioned 300 µm above the deeper viral injection site. A thin layer of Metabond was applied on the skull surface to secure the fiber. In addition, a thick layer of black dental cement was applied to secure the fiber implant for 1P illumination to allow positioning and restraint of the animal.

One week following AAV injection of the virus mixture, baseline signals were recorded with fiber photometry for 10 min in the home cage. A detailed description of the system can be found elsewhere[62]. After recordings, mice were connected to a 447-nm laser (Opto Engine) using a 200-µm optical fiber, illuminated with 5-mW, 100-ms pulses, at 1 Hz for 30 min (transistor–transistor logic-controlled by OTPG_4, Doric Lenses), in the home cage. A week following light exposure, fiber photometry signal was recorded again for 10 min. Fiber photometry peak detection was performed with MATLAB (R2018a), using the 'findpeaks' function and a prominence of 2.5. Mice were perfused 4 weeks after illumination.

Animals were perfused with 4% PFA. Brains were dissected and postfixed in 4% PFA overnight at 4 °C. Brains were then rinsed briefly with PBS and then sectioned at a thickness of 100 µm on a vibratome (VT1200, Leica Biosystems).

Fluorescent images from brain tissue were acquired with an LSM 880 confocal microscope (Carl Zeiss). We used a ×10 Plan Apochromat air objective (NA 0.45), a ×25 Plan Apochromat water immersion objective (NA 1.2) and three laser wavelengths (488, 561 and 633 nm). Image acquisition was controlled by Zen 2011 software (Zeiss), which also allowed automated tiling and maximum intensity projection. Images were not further processed. Expression counts were done by summation of the values of the fluorescence within 1×1 mm^2 below the fiber tip, subtracted with the same area at the opposite hemisphere, line by line, and normalized to the maximal value.

Zebrafish experiments. All experiments were performed in compliance with the University of Washington Institutional Animal Care and Use Committee. NCreV and CCreV were PCR amplified from pAAV-Ef1a NCreV and pAAV-Ef1a CCreV, and cloned into the pDest-ubi vector (Addgene plasmid no. 27323) by Gibson assembly. The pDest-ubi:N-vCre-pDest and pDest-ubi:C-vCre mixture containing equal amounts of each plasmid (25 pg each) and tol2 transposase RNA (25 pg) was injected into one-cell-stage tg(ubi:Zebrabow-M) zebrafish embryos. Embryos were either light or dark reared for 72 h. At 3 d postfertilization, injected embryos were anesthetized with Mesab, mounted in 2% agarose and imaged on a Zeiss LSM 880 confocal microscope.

fMOST imaging and reconstructions. All tissue preparation has been described previously[63]. Following fixation, each intact brain was rinsed three times (6 h for two washes and 12 h for the third wash) at 4 °C in 0.01 M PBS solution (Sigma-Aldrich). The brain was subsequently dehydrated via immersion in a graded series of ethanol mixtures (50%, 70% and 95% (vol/vol) ethanol solutions in distilled water) and the absolute ethanol solution three times for 2 h each at 4 °C. After dehydration, the whole brain was impregnated with Lowicryl HM20 Resin Kits (Electron Microscopy Sciences, cat. no. 14340) by sequential immersions in 50%, 75%, 100% and 100% embedding medium in ethanol, 2 h each for the first three solutions and 72 h for the final solution. Finally, each whole brain was embedded in a gelatin capsule that had been filled with HM20 and polymerized at 50 °C for 24 h.

The whole-brain imaging was performed using an fMOST system. The basic structure of the imaging system is the combination of a wide-field upright epi-fluorescence microscope with a mechanic sectioning system. This system runs in a wide-field block-face mode but is updated with a new principle to get better image contrast and speed, thus enabling high-throughput imaging of the fluorescence protein-labeled sample (manuscript in preparation, Q.L. et al.). Each time, we do a block-face fluorescence imaging across the whole coronal plane (x–y axes), then remove the top layer (z axis) by a diamond knife, then expose next layer and image again. The thickness of each layer is 1.0 µm. In each layer imaging, we used a strip scanning (x axis) model combined with a montage in the y axis to cover the whole coronal plane[64]. The fluorescence, collected using a microscope objective, passes a bandpass filter and is recorded with a time delay integration charge-coupled device camera. We repeat these procedures across the whole sample volume to get the required dataset.

The objective used is ×40 water immersion with NA 0.8 to provide a designed optical resolution (at 520 nm) of 0.37 µm in the x–y axes. The imaging gives a sample voxel of $0.30 \times 0.30 \times 1.0$ µm^3 to provide proper resolution to trace the neural process. The voxel size can be varied upon different objectives. Other imaging parameters for EGFP include an excitation wavelength of 488 nm, and emission filter with passing band of 510–550 nm. Three-dimensional reconstructions were performed manually using Neurolucida 360 (NL360).

Cortical targeted in vivo 2P stimulation of single cells. For in vivo targeted single-cell optogenomic modifications as well as simultaneous GCaMP7f imaging experiments, Stanford Administrative Panel on Laboratory Animal Care approved all animal procedures. Ai14 mice (The Jackson Laboratory, 07908) aged 2–4 months were used for experiments. For viral vector injection, mice were anesthetized with isoflurane. iCreV virus AAV2/PHP.eB-EF1a-iCreV, EGFP virus AAV2/PHP.eB-CAG-EGFP and GCaMP virus AAV2/9-CamkIIa-jGCaMP7f were used in all experiments. Viral vectors were loaded into glass pipettes and injected into cortices with a Picospritzer (Paker Hannifin). Approximately 500 nl of the virus solution was delivered into somatosensory cortices over 15 min, and then a 4-mm craniotomy was made with the injection site at the center 30 min after the injection. Dura was removed followed by cover glass installation and sealing using ultraviolet-curable adhesive Loctite 4305. A custom-made head bar and cover were secured with dental cement on the mouse skull. Imaging experiments started 1 month after the surgery to allow gene expression.

The mouse was mounted on a running wheel with head fixation and remained awake during the whole experiment. Before imaging, the head mount cover was removed. To operate the mouse and the microscope, a red LED light was used for illumination (Wayllshine). Ultrasound gel (Parker, Aquasonic) was put on the cover glass for the water immersion objective lens. The mouse was aligned manually without checking the focal plane with the eye piece to avoid iCreV induction during this process.

For induction experiments, a femtosecond Ti:sapphire laser (Spectra-Physics, Mai Tai) was tuned to 920-nm wavelength. The scanning and image acquisition were achieved with a Prairie (Bruker) 2P microscope, through a ×20 0.95 NA water immersion lens (Olympus XLUMPLFLN-W 0.95 NA 20×). For all of the imaging sessions, laser power at a specimen was kept at 25 mW and it was monitored (Thorlabs, PM100D and S130C) at an additional output of the optical path before entering the microscope, of which a splitting ratio was calibrated before the measurements. During the first imaging session, a starting point with unique vessel pattern was identified and recorded. All target cells' relative coordinates to the starting position were recorded and used for relocation in later sessions. Images were acquired with 4-µs pixel dwell time at $1{,}024 \times 1{,}024$ pixel frame size (field of view 450×450 µm^2), with 3-µm z axis step size. After identifying a target cell, an induction scanning was carried out using the region of interest function to limit the scanning of the middle of the target cell's somata region. The scanning pixel dwell time was increased to 10 µs and various scanning conditions were used in each mouse tested. After the first induction session, the head cover was re-installed to seal the craniotomy from ambient light. At 7–10 d after the first session, all of the cells were re-imaged to check tdTomato expression and at the end underwent a 30-min blue LED exposure (5 mW, 470 nm, Thorlabs, M470L3). The third imaging session was carried out 7–10 d after the LED exposure.

For the calcium imaging experiment, a custom-made 2P microscope was used with objective lens Olympus XLUMPLFLN-W 0.95 NA ×20 and 8-kHz resonant scanner head (Cambridge Technologies, CRS8K/6215H). Fluorescence light was captured using H11706-40 and H10770PA-40 photomultiplier tubes equipped with low-noise amplifiers (Femto, DHPCA-100), with their analog signal subsequently digitized (National Instruments, NI-5732) and formed into images using a field programmable gate array (National Instruments, FPGA NI-7961R) and ScanImage software (Vidrio Technologies)[65]. GCaMP7f signal was collected at 30-Hz frame repetition rate for 30 min in each mouse.

Reporting Summary. Further information on research design is available in the Nature Research Reporting Summary linked to this article.

Data availability

DNA sequences of the NCreV, CCreV, NDreV, CDreV, iCreV, iDreV and iFlpV created in this work are curated in National Institute of Health, GenBank. Accession codes are NCreV, MT036266; CCreV, MT036267; NDreV, MT036268; CDreV, MT036269; iCreV, MN944913; iFlpV, MN944914; and iDreV, MN944915. AAV iCreV, 140135; AAV iDreV, 140136; AAV iFlpV, 140137; AAV NCreV, 140131; AAV CCreV, 140132; AAV NDreV, 140134; and AAV CDreV, 140133. Plasmids have been deposited in Addgene with the indicated accession codes. All in vivo and in vitro raw data images used in all figures presented in the paper are available from the corresponding author upon request. Source data files for all figures with graphs are provided in raw tabular form as Excel files.

Code availability

The two-photon microscope was operated using ScanImage v.5.3 (Vidrio Technologies, LLC) software and custom software written in LabView 2015 (National Instruments). The code is available upon request to the authors.

References

60. Cetin, A., Komai, S., Eliava, M., Seeburg, P. H. & Osten, P. Stereotaxic gene delivery in the rodent brain. *Nat. Protoc.* **1**, 3166–3173 (2006).
61. Franklin, K. B. J. & Paxinos, G. *The Mouse Brain in Stereotaxic Coordinates* 18th edn (Academic Press, 1997).
62. Cho, J. R. et al. Dorsal Raphe dopamine neurons modulate arousal and promote wakefulness by salient stimuli. *Neuron* **94**, 1205–1219.e1208 (2017).
63. Gang, Y. et al. Embedding and chemical reactivation of green fluorescent protein in the whole mouse brain for optical micro-imaging. *Front. Neurosci.* **11**, 121 (2017).
64. Li, A. et al. Micro-optical sectioning tomography to obtain a high-resolution atlas of the mouse brain. *Science* **330**, 1404–1408 (2010).

65. Pologruto, T. A., Sabatini, B. L. & Svoboda, K. ScanImage: flexible software for operating laser scanning microscopes. *Biomed. Eng. Online* **2**, 13 (2003).

Acknowledgements

We are grateful to the Structured Science teams at the Allen Institute for technical support with stereotaxic injections and mouse colony management. The work was funded by the Allen Institute for Brain Science; NIMH BRAIN Initiative grant no. RF1MH114106 to A.Cetin; the NSFC Science Fund for Creative Research Group of China (grant 61721092) to H.G., Q.L. and S.Z.; NIH Brain Initiative grant no. RF1MH117069 to V.G.; the Colvin divisional fellowship of the Division of Biology and Biological Engineering, California Institute of Technology, to A.K.; and NIH BRAIN Initiative grant U01NS107610 to M.S. The creation of the Ai139 mouse line was supported by NIH grant no. R01DA036909 to B.T. We thank S. Durdu, H. Bayer, D. Schrom, B. Kerman and K. Yonehara for critical reading and feedback. We thank the Allen Institute founder, P.G. Allen, for his vision, encouragement and support.

Author contributions

A. Cetin conceptualized the light-inducible recombinase system. S.Y. performed cloning and characterization of the constructs and participated in image acquisition. B.O. and P.B. performed surgeries, immunohistochemistry and image acquisition. T.Z. Performed cloning. M.M. performed some of the surgeries and light stimulations. T.L.D. performed some of the initial cloning experiments. B.T. and H.Z. contributed to the generation of the Ai139 transgenic mice. H.G., Q.L. and S.Z. acquired fMOST data. X.K. and Y.W. performed Neurolucida reconstructions. V.G. and A.K. designed deep brain imaging experiments and generated the associated data, figure and text. A.K. performed deep brain imaging experiments. S.C. and P.B. performed 2P-induced recombination experiments. A. Curtright and A.D. performed zebrafish experiments. R.C., P.Y. and M.S. performed targeted single-cell 2P experiments and combinatorial cortical jGCaMP7F calcium imaging experiments. A. Cetin and H.Z. designed and coordinated the study, and wrote the manuscript with inputs from all co-authors.

Competing interests

The authors declare no competing interests.

Additional information

Supplementary information is available for this paper at https://doi.org/10.1038/s41592-020-0774-3.

Correspondence and requests for materials should be addressed to A.C.

Peer review information Nina Vogt was the primary editor on this article and managed its editorial process and peer review in collaboration with the rest of the editorial team

nature research

Corresponding author(s): Ali Haydar Cetin

Last updated by author(s): February 6, 2020

Reporting Summary

Nature Research wishes to improve the reproducibility of the work that we publish. This form provides structure for consistency and transparency in reporting. For further information on Nature Research policies, see Authors & Referees and the Editorial Policy Checklist.

Statistics

For all statistical analyses, confirm that the following items are present in the figure legend, table legend, main text, or Methods section.

n/a	Confirmed	
☐	☒	The exact sample size (*n*) for each experimental group/condition, given as a discrete number and unit of measurement
☐	☒	A statement on whether measurements were taken from distinct samples or whether the same sample was measured repeatedly
☒	☐	The statistical test(s) used AND whether they are one- or two-sided *Only common tests should be described solely by name; describe more complex techniques in the Methods section.*
☒	☐	A description of all covariates tested
☒	☐	A description of any assumptions or corrections, such as tests of normality and adjustment for multiple comparisons
☐	☒	A full description of the statistical parameters including central tendency (e.g. means) or other basic estimates (e.g. regression coefficient) AND variation (e.g. standard deviation) or associated estimates of uncertainty (e.g. confidence intervals)
☒	☐	For null hypothesis testing, the test statistic (e.g. *F*, *t*, *r*) with confidence intervals, effect sizes, degrees of freedom and *P* value noted *Give P values as exact values whenever suitable.*
☒	☐	For Bayesian analysis, information on the choice of priors and Markov chain Monte Carlo settings
☒	☐	For hierarchical and complex designs, identification of the appropriate level for tests and full reporting of outcomes
☒	☐	Estimates of effect sizes (e.g. Cohen's *d*, Pearson's *r*), indicating how they were calculated

Our web collection on statistics for biologists contains articles on many of the points above.

Software and code

Policy information about availability of computer code

Data collection	Cell counting and quantification of relative fluorescence intensity were performed by ImageJ. Zeiss microscope is operated through the commerical software Zen (2.6). fMOST images were reconstructed using Neurolucida (Neurolucida 360 or NL360). Two-photon images were collected through Prairie View (1.4) and Scan Image (5.6) softwares.
Data analysis	Figures were prepared in Adobe Illustrator CC. Boxplots and dot plots were prepared in RStudio. Images were analyzed with manual inspection facilitated by ImageJ. For counting labeled cells, a segmentation plug-in Weka (3.2.33) is trained and applied to the dataset, with manual inspection of the results.

For manuscripts utilizing custom algorithms or software that are central to the research but not yet described in published literature, software must be made available to editors/reviewers. We strongly encourage code deposition in a community repository (e.g. GitHub). See the Nature Research guidelines for submitting code & software for further information.

Data

Policy information about availability of data

All manuscripts must include a data availability statement. This statement should provide the following information, where applicable:

- Accession codes, unique identifiers, or web links for publicly available datasets
- A list of figures that have associated raw data
- A description of any restrictions on data availability

All relevant plasmids will be deposited to Addgene. Data are available from the corresponding author upon request.

Field-specific reporting

Please select the one below that is the best fit for your research. If you are not sure, read the appropriate sections before making your selection.

☒ Life sciences ☐ Behavioural & social sciences ☐ Ecological, evolutionary & environmental sciences

For a reference copy of the document with all sections, see nature.com/documents/nr-reporting-summary-flat.pdf

Life sciences study design

All studies must disclose on these points even when the disclosure is negative.

Sample size	No statistical methods were used to predetermine sample size. For the in vivo single cell two-photon experiments, three pilot tests of the CreV infection and induction were performed to gauge the appropriate laser power and induction time. The sample size during the single cell induction experiment was not predetermined since it depended completely on the infection efficiency and spread. The sample size is sufficient in demonstrating different induction condition showed different success rate. And for the spatial specificity (which is an important aspect of the experiment) has plenty of samples (>100) for each conditions.
Data exclusions	No animals were excluded from analysis. For all the in vivo single cell two-photon experiments, no data is excluded.
Replication	All in vitro experiments show four replicas (Figure 1, Supp Fig 3 and 5) . For in vivo experiment of different RecV systems (Figure 2, Supp Fig 4, 6, 7, 8 and 9), each experiment has two replicas. For zebra fish experiments, total 61 embryos were used for injections (Figure 3). For in vivo targeted 2P induction experiment (Figure 5, Supp Fig 10 and 11), the experiments have been reproduced in total 8 mice.
Randomization	It was not necessary to randomize the grouping of animals since our comparisons focused on the same animal before and after 2P stimulation and on areas of the same brain with differential exposure to light. In the in vivo single cell two-photon experiments, individual cells' assignment to different induction conditions were randomized. No correlation exist between the depth of cell and the condition of conversion (as shown in supplementary figure)
Blinding	Investigators were not blind to groups since different groups of animals received different conditions of light exposures. In the in vivo single cell two-photon experiments, the analysis of induction was done without the knowledge of cell/condition assignment and was grouped into each condition group post-hoc.

Reporting for specific materials, systems and methods

We require information from authors about some types of materials, experimental systems and methods used in many studies. Here, indicate whether each material, system or method listed is relevant to your study. If you are not sure if a list item applies to your research, read the appropriate section before selecting a response.

Materials & experimental systems

n/a	Involved in the study
☐	☒ Antibodies
☐	☒ Eukaryotic cell lines
☒	☐ Palaeontology
☐	☒ Animals and other organisms
☒	☐ Human research participants
☒	☐ Clinical data

Methods

n/a	Involved in the study
☒	☐ ChIP-seq
☒	☐ Flow cytometry
☒	☐ MRI-based neuroimaging

Antibodies

Antibodies used	anti-Somatostatin-28, T-4546.0400, Peninsula Laboratories, CA, USA
Validation	The staining pattern in somatostatin-cre link matched the characteristics of somatostatin neurons.

Eukaryotic cell lines

Policy information about cell lines

Cell line source(s)	HEK293T cells from ATCC {CRL-11268)
Authentication	Morphology check by microscope, Growth curve analysis, Species verification by Isoenzymology, Identity verification with STR analysis (DNA fingerprinting)
Mycoplasma contamination	This cell line was tested negative for mycoplasma contamination

Commonly misidentified lines (See ICLAC register)	None

Animals and other organisms

Policy information about studies involving animals; ARRIVE guidelines recommended for reporting animal research

Laboratory animals	Adult mice {C57BL/6J, Ai14, Ai75, Ai66R, and Ai65F reporter line, Rbp4-Cre and Sst-Flpo transgenic lines) with 2-4 months age of both genders and zebrafish embryos were used for injections and 3 dpf larvae were used for imaging in this study.
Wild animals	No wild animals were used in this study.
Field-collected samples	No field-collected samples were used in this study.
Ethics oversight	Animal experiments were performed according to the guidelines of the Allen Institute for Brain Sciences, California Institute of Technology, Stanford University, and University of Washington.

Note that full information on the approval of the study protocol must also be provided in the manuscript.